Comparison of Artificially Rough Surface with the Smooth Surface Solar Air Heater Using FEA

Rakesh Singh[1], Prof K.K. Jain[2]
[1] *Research Scholar, Department of Mechanical Eng. SRIT, Jabalpur, (M.P.)*
[2] *Prof, Department of Mechanical Eng. SRIT, Jabalpur, (M.P.)*

Abstract- **Usually, conventional solar air heater has very low thermal performance due to the smooth absorber plate offers low convective heat transfer to moving air, leading to high heat losses to atmosphere. The working of solar air heater may be improved via mainly two methods: 1. reducing the top heat losses to atmosphere, 2 increasing the convective heat transfer coefficients at absorber plate. Second methods is the most common due to its extensive applicability**

A Finite Element Analysis of artificial roughness geometry of V rib type in the absorber plate of solar air heater duct has been carried out and compared with smooth duct. A comparative Finite element analysis has been carried out for air at different velocity (inlet) and temperature of fluid for both absorber plate surfaces. The outcomes of the present Finite Element analysis represents the artificial roughened surface is more suitable then the flat plate surface solar air heater.

The objective of the present study is to make the comparative study of flat surface solar air heater with an artificially roughened surface solar air heater on the basis of

- **Varying fluid inlet temperature**
- **Varying fluid inlet velocity**

Index Terms- **Artificial roughness, solar air heater, heat transfer co-efficient, FEA etc.**

1. INTRODUCTION

1.1 General

In the present world, the prosperity of a nation is measured by the energy consumption of that nation and the GDP of a country is directly linked with energy consumption. Therefore, the demand for energy resources is increasing day by day. There are various forms of energy resources, but they are divided into two main forms, renewable energy resources (solar, air, wind) and non-renewable energy resources (coal and petroleum). The industrial growth is accelerated by non-renewable energy resources, but the stock is limited in nature. The rapid depletion of fossil fuel resources has necessitated an urgent need for alternative energy sources in order to meet the energy demands of the immediate future and the generations to come. Among the many alternatives, solar energy stands out as the brightest and long range promise towards meeting the continually increasing demand for energy.

A solar thermal collector is a heat exchanger that converts radiant solar energy into heat. In essence this consists of a receiver that absorbs the solar radiation and then transfers the thermal energy to a working fluid. Because of the nature of the radiant energy (its spectral characteristics, its diurnal and seasonal variability, changes in diffuse to global fraction, etc.), as well as the different types of applications for which solar thermal energy can be used, the analysis and design of solar collectors present unique and unconventional problems in heat transfer, optics, and material science. The classification of solar collectors can be made according to the type of working fluid (water, air, or oils) or the type of solar receiver used (non-tracking or tracking).

1.2 Solar Thermal Heat Utilization

Part of the solar radiation energy can be converted into heat by using absorbers (e.g. solar collectors. The absorbers together with the other essential segments are the close planetary system. Heavenly bodies are establishments changing over sun powered radiation into warm with a specific end goal to warm swimming pools, deliver residential high temp water, cover the interest for space warming or supply other warmth shoppers.

1.3 Role of artificial roughness

Generally, thermal performance of smooth absorber plate is considered to be low because of low convective heat transfer coefficient. Sub laminar layer is developed over absorber plate which acts as thermal resistant to flowing air. For enhancing the heat transfer rate, sub laminar layer is broken/disturbed by creating local turbulence which is achieved using artificial roughness. Artificial roughness are created underside of absorber plate by means of small height wires attached to absorber plate in repeated nature.

2 LITERATURE REVIEW

Studies have been carried out in different absorber plate solar air heaters, some of them are as:

1. *"Nusselt number and friction factor correlations for forced convective type counter flow solar air heater having discrete multi V shaped and staggered rib roughness on both sides of the absorber plate",* 2017, Ravi Kant Ravi, R.P. Saini, Applied Thermal Engineering (2017)

In this work, the consequences of an exploratory examination on warm exchange and rubbing factor in a counter stream twofold pass sunlight based air warmer (DPSAH) channel with discrete multi V-formed and amazed rib unpleasantness on two wide surfaces of the warmed plate have been researched. The examination covers an extensive variety of Reynolds number (Re) from 2000 - 20000, relative amazed rib pitch (p'/p) from 0.2– 0.8, relative stunned rib measure (r/e) from 1– 4 and relative unpleasantness width (W/w) from 5-8. The ideal estimations of stream and geometrical parameters of harshness have been achieved and clarified in detail.

2. *"A critical review on artificial roughness provided in rectangular solar air heater duct"*, 2017 Tabish Alam, Man-Hoe Kim, Renewable and Sustainable Energy Reviews 69 (2017) 387–400

Utilizations of fake harshness on the underside of safeguard plate in sun based air warmer pipe have been broadly used to enhance warm exchange with direct increment of grating variable. The outline of the harshness shape and game plan is most vital to upgrade the roughened surfaces. The unpleasantness parameters and ribs plan are capable to modify the stream structure and warmth exchange instruments are essentially represented by stream structure. The basic audits on different simulated unpleasantness components accessible in writing have been led and the impacts of the harshness designs are examined. The Nusselt number and grating element connections for different harshness components have been abridged. A correlation investigation of thermo-pressure driven execution of various harshness components has likewise been accounted for to comprehend the consequences of utilizations of simulated unpleasantness.

3. *"Performance prediction for solar air heater having rectangular sectioned tapered rib roughness using CFD",* 2017, L. Varshney, A.D. Gupta

In the present work CFD analysis of a solar air heater (SAH) duct provided with artificial roughness in the form of rectangular sectioned tapered rib has been performed using Ansys FLUENT. Twelve different configurations of tapered rib with taper angle, of 1.6°, 2.3° and 3.2° for pitch of 10,15,20 and 25 mm and constant rib width, wr=0.7 mm have been considered as roughness element. A three-dimensional non-uniform hybrid grid is generated according to the configuration using cutcell method. The differential equations involved in the model are solved with a finite-volume-based numerical method. The RNG k turbulence model with enhanced wall function is used to solve the transport equations for turbulent flow and energy dissipation rate. Effect of roughness parameters namely tapered angle and relative roughness pitch on Nusselt number and friction factor for a constant value of heat flux (1000 W/m^2) is discussed. The optimal values of geometrical parameters are obtained on the basis of the performance index in the range of Reynolds number 3800 to 18000. Optimum performance index is found to be 1.91 corresponding to the 1.6° and relative roughness pitch, P/e of 10.7 at Reynolds number, Re of 12,000.

3 RESEARCH METHODOLOGIES

3.1 Thermal performance of solar air heater

Performance of any system signifies the degree of utilization of input to the system. It is essential to

investigate thermal and hydraulic performance of a solar air heater for making an efficient design of such type of a system. Thermal performance concerns with heat transfer process with in the collector and hydraulic performance concerns with pressure drop in the duct. A Conventional solar heater is considered for the study.

Thermal concert of a solar air heater can be calculated with the use of *Hottel–Whillier–Bliss equation presented* by *Duffie and Beckman*

$$Q_u = A_c F_R [I (\tau\alpha)_e - U_L(T_i - T_a)] \quad . (3.1)$$

The proportion of useful energy gain through the moving air by duct of a solar air heater may also be considered by using the following relations:

$$Q_u = mC_p(T_o - T_i)$$

Where

Ac surface area of absorber plate, m^2

F_R heat removal factor

I intensity of solar radiation, W/m^2

(τα)e effective transmittance-absorptance product

U_L overall heat loss coefficient, W/m^2 K

T_i fluid inlet temperature, K

T_a ambient temperature, K

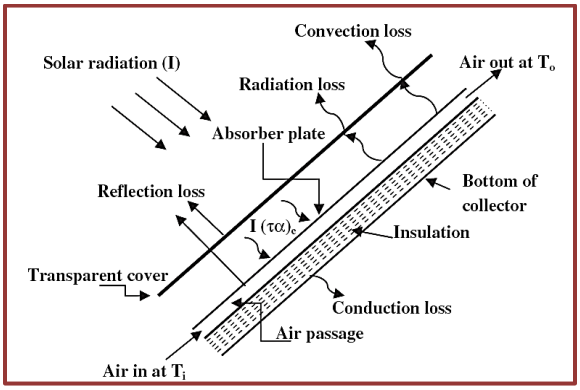

Figure 3.1 Solar Air Heater Principle

The heat transfer coefficient (h) can be improved via applying artificial roughness on the surface of absorber plate. It can be signified in non-dimensional form via expending the following relationship of Nusselt number (Nu) described by Duffie and Beckman

Where Ac is the surface area of absorber plate (m^2) F_R is the Heat removal Factor, I is the turbulence intensity/intensity of solar radiation (W/m^2), $(\tau\alpha)_e$ is the effective transmittance absorptance product, U_L is the overall heat loss coefficient ($W/m^2/K$), Ti fluid inlet temperature (K) and Ta ambient temperature (K).

The three design factors, F_R, $(\tau\alpha)_e$, and U_L, are events of thermal performance and syndicate to yield complete collector efficiency in terms of the operating variables of temperature and insolation. The three factors can be used to identify features which would enhance performance with the highest cost-benefit. Conversely, factors that are not economically justifiable in improving performance may be eliminated to reduce costs.

Heat removal factor is known as,

$$Heat\ Removal\ factor\ F_R = \frac{Usefull\ Energy}{Using\ Energy} = \frac{T_i - T_a}{T_{pm} - T_a}$$

The rate of valuable energy gain by flowing air in the duct of a solar air heater can also be calculated from the following equation

$$Q_u = mC_p(T_0 - T_i) = hA_c(T_{pm} - T_{am}) \quad . (3.2)$$

The overall heat loss Q_L from the air heater is a summation of the losses from the surfaces of top, back, and edge of the collector. The overall loss coefficient is well-defined as *(Rajendra Karwa et al)*

$$U_L = \frac{Q_L}{A(T_{pm} - T_a)} \quad . (3.3)$$

The heat transfer over the glass shield of thickness δ by conduction is

$$Q_{tg} = \frac{K_g A(T_{gi} - T_{go})}{\delta} \quad . (3.4)$$

Where Kg is the thermal conductivity of the glass and Tgo is temperature of the outer surface of the glass cover. The back loss from the collector can be calculated from the following equation:

$$Q_b = \frac{A\,(T_b - T_a)}{(\delta/K_i + 1/h_w)} \quad . (3.5)$$

Where δ is the insulation thickness, ki is the thermal conductivity of the insulating material and Tb is the temperature of the bottom surface of the collector duct. h_w is the wind heat transfer coefficient. *McAdams (1954)* reported a correlation, based on experimental data of Jurges, between wind induced convective heat transfer coefficient and wind speed as

$$h_w = 5.7 + 3.8\,V_w \quad (3.6)$$

Where Vw is the wind velocity. For the estimate of the edge loss, the empirical equation suggested by *Klein* can be used, which is given by

$$Q_e = 0.5\,A_e\,(T_p - T_a) \quad . (3.7)$$

Where Ae is the area of the edge of the air heater rejecting heat to the surroundings. Further, thermal

efficiency of a solar air heater can be expressed by the following equation;

$$\eta_{th} = \frac{Q_u}{IA} \quad . (3.8)$$

A flat-plate solar collector usually has a non-selective or a selective black plate with one or two glass covers a few centimeters above the black plate, and a well-insulated back. The length of the plate is typically about 2m. Edge effects are usually small.

The transmittance $\tau(\theta)$ of a glass cover for solar radiation depends on the angle of incidence θ. Typical values for clear glass are given in Table 3.1.

Table 3.1 Transmittance of a Glass Cover.

θ:	0°	60°	70°	80°	90°
$\tau(\theta)$:	0.9	0.8	0.65	0.35	0

The absorptance $\alpha(\theta)$ of the black plate for solar radiation also depends on the angle of incidence θ. Table 3.2 shows typical values for $\alpha(\theta)$ and the product $\tau(\theta).\alpha(\theta)$.

Table 3.2 Absorptance of a Black Plate

θ:	0°	60°	70°	80°	90°
$\alpha(\theta)$:	0.92	0.85	0.75	0.60	0
$\tau(\theta).\alpha(\theta)$:	0.83	0.68	0.49	0.21	0

3.4 Hydraulic performance

Hydraulic performance of a solar air heater disquiets with pressure drop (ΔP) in the duct. Pressure drop totals for energy consumption by blower to propel air concluded the duct. The pressure drop for completely established turbulent flow through duct with Re 50,000 is given as follows equation:

$$\Delta P = \frac{2f\rho l v^2}{D} \quad . (3.9)$$

$$f = 0.079\ Re^{-0.25} \quad . (3.10)$$

Where v is the velocity of air in the duct (m/s), f is the friction factor, ρ is the density of air (kg/m^3), D is the equivalent or hydraulic diameter of duct (m) and l is the length of the duct.

3.5 Finite Element Analysis

Computational fluid dynamics or CFD is the learning of systems regarding fluid flow, heat transfer and related occurrences similar as chemical reactions via resources of computer-based simulation.

A two-dimensional CFD simulation of artificially roughened solar air heater is carried out using the CFD software package ANSYS FLUENT (version 15.1) that uses the finite-volume method to solve the governing equations.

Computational fluid dynamics (CFD) is the discipline of responsible a numerical solution to the governing equations of fluid flow whilst advancing the solution through space or time. This approach (CFD) is used in various applications similar as aerospace, automotive biomedical, chemical processing, HVAC, hydraulics, marine, oil and gas, power generation and sports. The use of computational approach (CFD) mainly taken into concern when physics is well captured in a set of governing relations.

Pre-processor

Pre-processing consists of the input of a flow problem to a CFD program by means of an operator-friendly interface and the subsequent transformation of this input into a form suitable for use by the solver. The user activities at the pre-processing stage involve:

Definition of the geometry of the region of interest: the computational domain

Figure 3.2 shows the geometry of solar air heater using for the study. *The inclined ribs as shown in figure 3.2 is considered for the study*. The geometry is made using Auto CAD inventor and thus it is imported in Ansys Workbench.

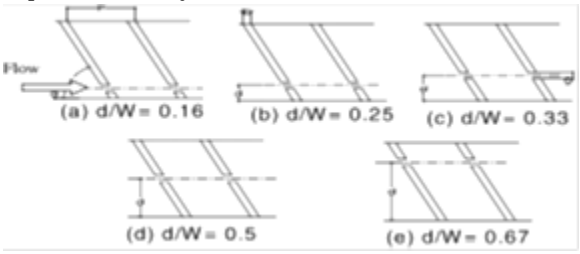

Figure 3.2 Inclined continuous ribs with gaps [T. Alam, M.-H. Kim]

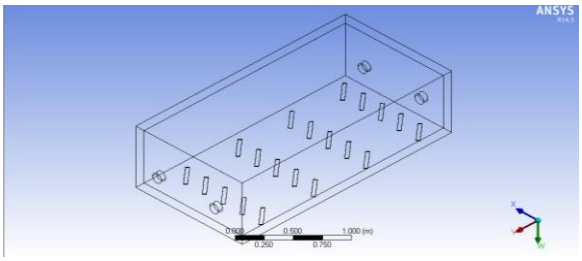

Figure 3.3 (a) Design Consideration for inclined ribs artificially roughened solar air heater (considering d/w =0.5)

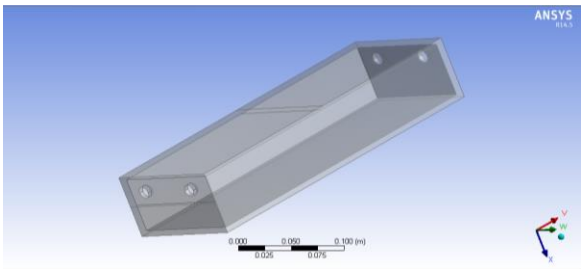

Figure 3.3 (b) Geometry of Flat surface absorber plate solar air heater used for the study.

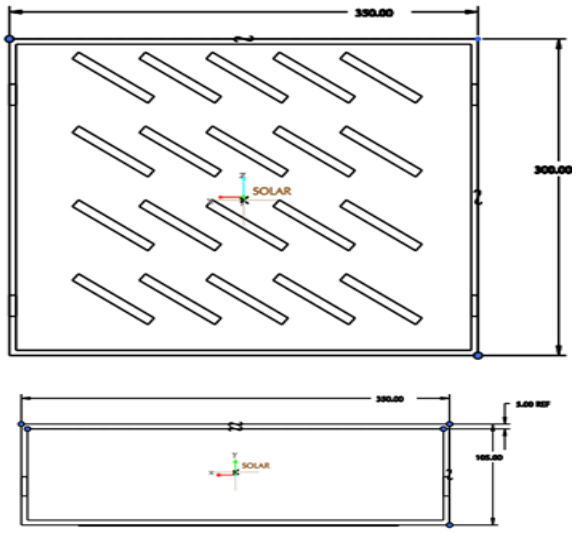

Figure 3.4 (a) Dimensional view of inclined rib solar air heater used for the study

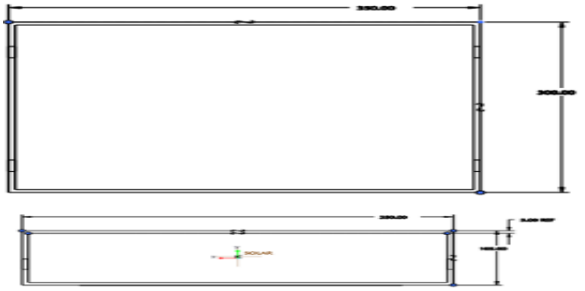

Figure 3.4 (b) Dimensional view of flat surface solar air heater used for the study

Table 3.3 Specification of Solar Air Heater

Overall length (m)	0.35
Overall height (m)	0.105
Absorber plate dimension (m)	0.35×0.3
Glass cover thickness (m)	0.005

Grid generation

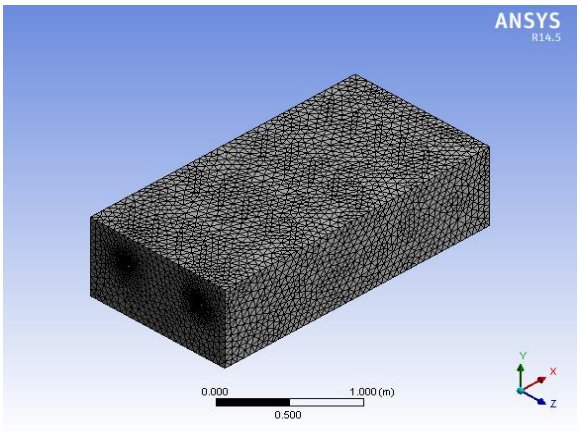

Figure 3.5 Mesh Generation for inclined ribs artificially roughened solar air heater

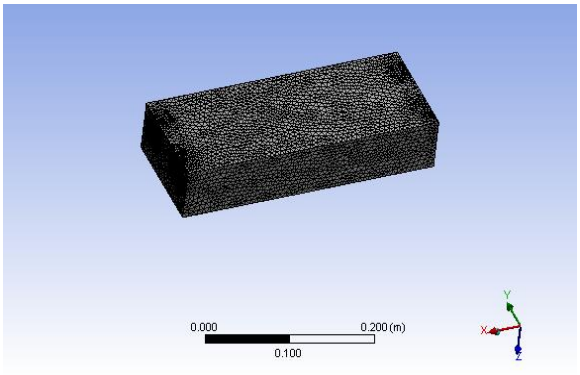

Figure 3.6 Mesh Generation for Flat surface absorber plate solar air heater

4 RESULT ANALYSES

The Finite element analysis has been carried out for the study. The analysis is carried out for comparing the two different Solar Air Heater (i.e. *solar air heaters with and without the artificial roughness*). The comparison has been carried out in two different ways, in first part the inlet temperature is considered as variable with constant wind velocity 0.5 m/s while in second part the wind velocity is considered as variable and inlet temperature is considered constant as 10°C.

4.1 Considering wind velocity constant and varying the inlet temperature

Figure 4.1 to 4.3 shows the distribution of temperature at different fluid inlet temperature varying from 0°C to 20°C at constant velocity 0.5 m/s for flat surface Solar air heater and figure 4.4 to 4.6 shows the same for artificial roughened solar air heater.

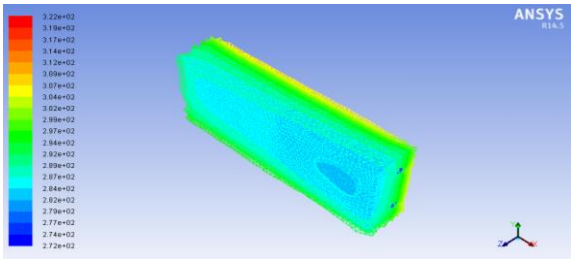

Figure 4.1 Temperature distribution while considering inlet temperature 0°C and 0.5 m/s velocity. (Flat Surface)

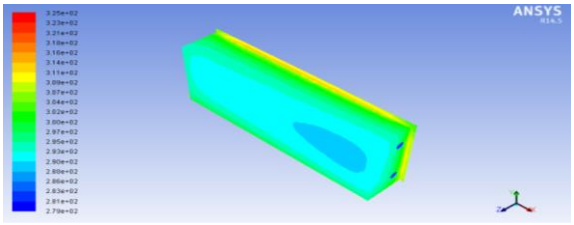

Figure 4.2 Temperature distribution while considering inlet temperature 10°C and 0.5 m/s velocity. (Flat Surface)

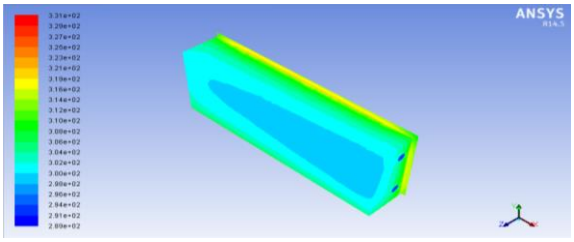

Figure 4.3 Temperature distribution while considering inlet temperature 20°C and 0.5 m/s velocity. (Flat Surface)

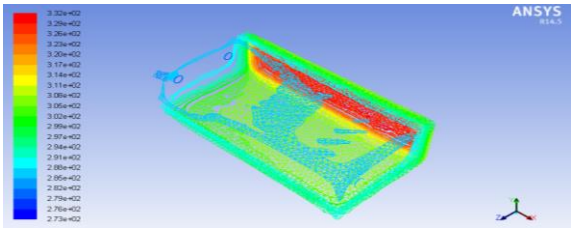

Figure 4.4 Temperature distribution while considering inlet temperature 0°C and 0.5 m/s velocity (art roughened surface)

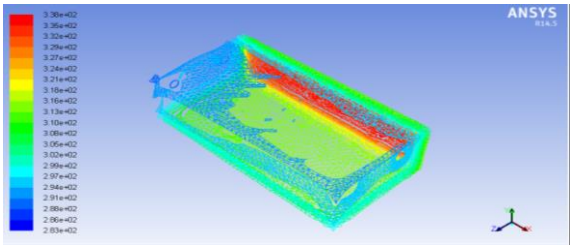

Figure 4.5 Temperature distribution while considering inlet temperature 10°C and 0.5 velocity (art roughened surface)

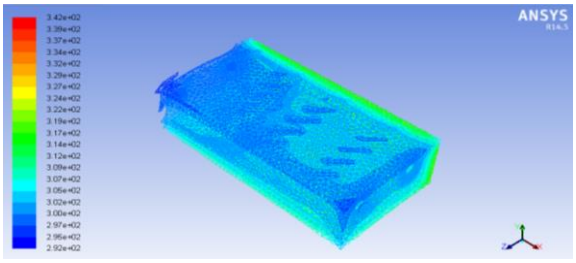

Figure 4.6 Temperature distribution while considering inlet temperature 20°C and 0.5 velocity (art roughened surface)

Table 4.1 Relation between Air outlet temperature and Air inlet temperature

Air Inlet temperature (K)	Air Outlet Temperature (K) (Art Roughened Surface)	Air Outlet Temperature (K) (Flat Plate Surface)
273	332	322
283	338	325
293	342	331

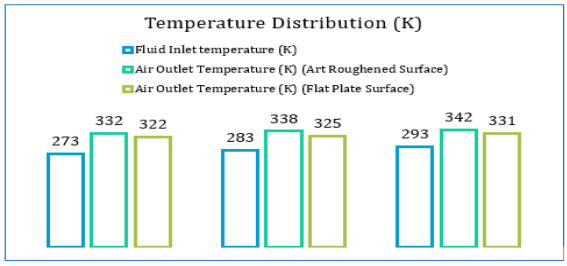

Figure 4.7 Difference in Air inlet and outlet temperature achieved for both the solar air heater

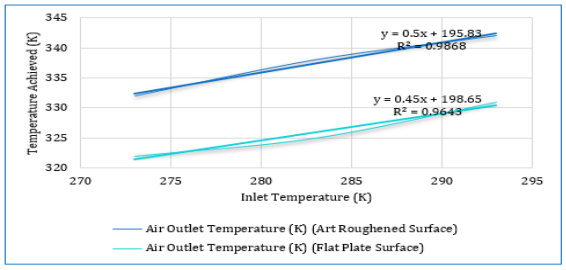

Figure 4.8 Relation between inlet and outlet temperature for both the solar air heater

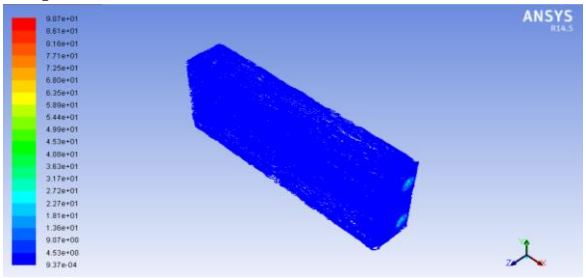

Figure 4.9 Turbulence distribution while considering inlet temperature 0°C and 0.5 velocity (flat plate surface)

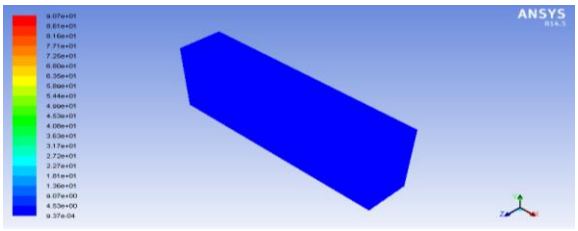

Figure 4.10 Turbulence distribution while considering inlet temperature 10°C and 0.5 velocity (flat plate surface)

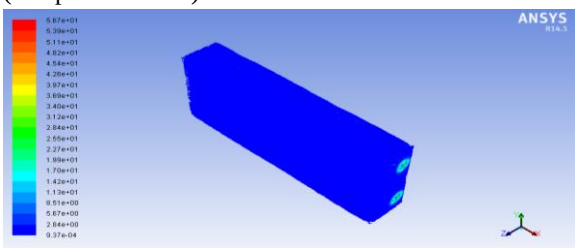

Figure 4.11 Turbulence distribution while considering inlet temperature 20°C and 0.5 velocity (flat plate surface)

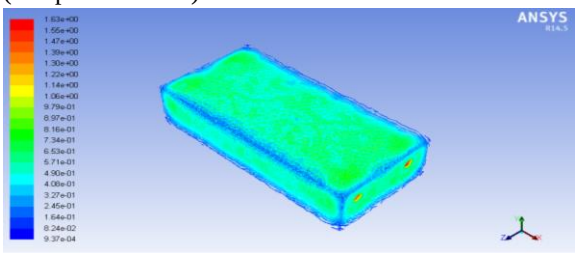

Figure 4.12 Turbulence distribution while considering inlet temperature 0°C and 0.5 velocity (art roughened surface)

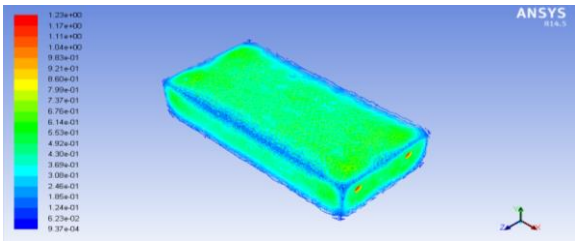

Figure 4.13 Turbulence distribution while considering inlet temperature 10°C and 0.5 velocity (art roughened surface)

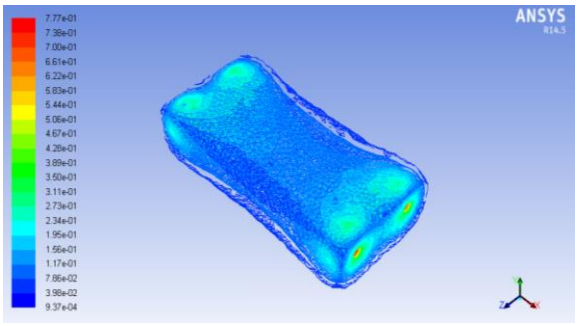

Figure 4.14 Turbulence distribution while considering inlet temperature 20°C and 0.5 velocity (art roughened surface)

Table 4.2 Relation between Turbulence (m^2/s^2) (for Art Roughened and flat plate Surface)and Air inlet temperature

Air Inlet temperature (K)	Turbulence (m^2/s^2) (Art Roughened Surface)	Turbulence (m^2/s^2) (Flat Plate Surface)
273	1.63	90.66
283	1.22	90.66
293	0.77	56.7

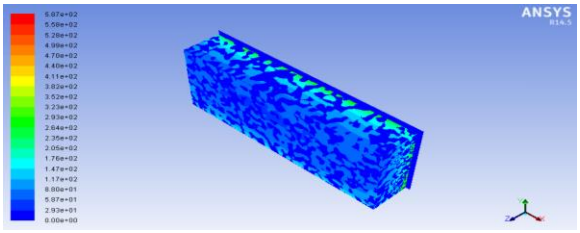

Figure 4.15 Solar Heat Flux distribution while considering inlet temperature 0°C and 0.5 velocity (Flat plate Surface)

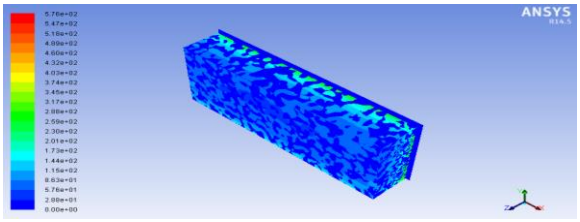

Figure 4.16 Solar Heat Flux distribution while considering inlet temperature 10°C and 0.5 velocity (Flat plate Surface)

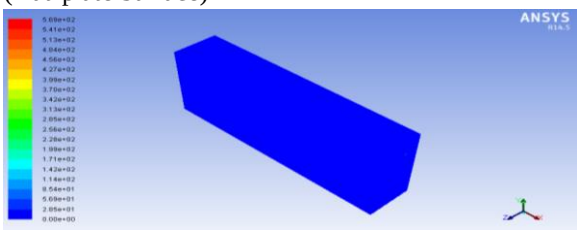

Figure 4.17 Solar Heat Flux distribution while considering inlet temperature 20°C and 0.5 velocity (Flat plate Surface)

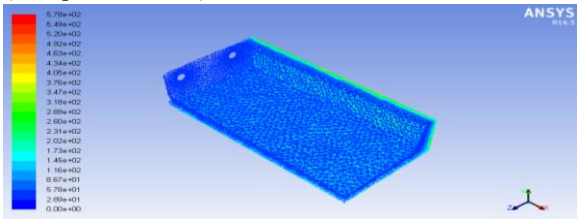

Figure 4.18 Solar Heat Flux distribution while considering inlet temperature 0°C and 0.5 velocity (art roughened surface)

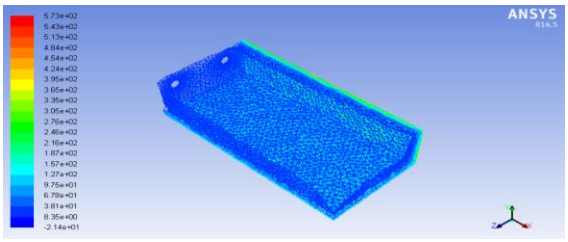

Figure 4.19 Solar Heat Flux distribution while considering inlet temperature 10°C and 0.5 velocity (art roughened surface)

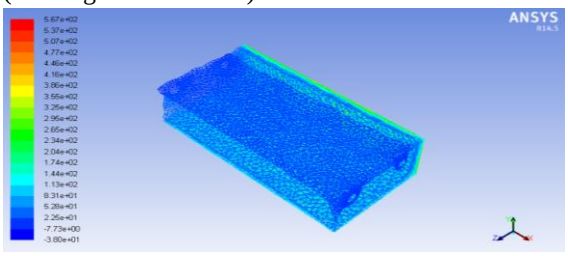

Figure 4.20 Solar Heat Flux distribution while considering inlet temperature 20°C and 0.5 velocity (art roughened surface)

Table 4.3 Relation between Radiation Heat Flux (W/m^2) (for Art Roughened and flat plate Surface) and Air inlet temperature

Air Inlet temperature (K)	Radiation Heat Flux (W/m^2) (Art Roughened Surface)	Radiation Heat Flux (W/m^2) (Flat Plate Surface)
273	578.298	586.98
283	572.82	575.56
293	567.313	569.45

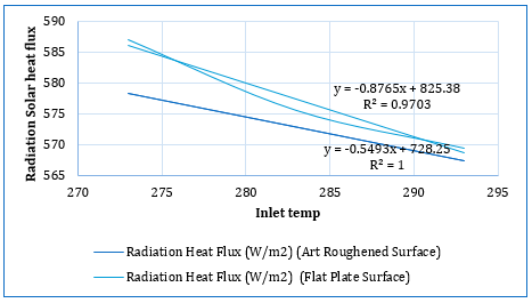

Figure 4.21 Radiative Solar Heat Flux distribution while considering inlet temperature varying from 0°C to 20°C and 0.5 velocity

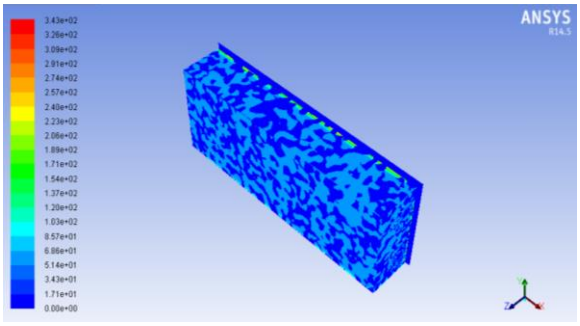

Figure 4.22 Absorbed Visible Solar Heat Flux distribution while considering inlet temperature 0°C and 0.5 velocity (flat plate surface)

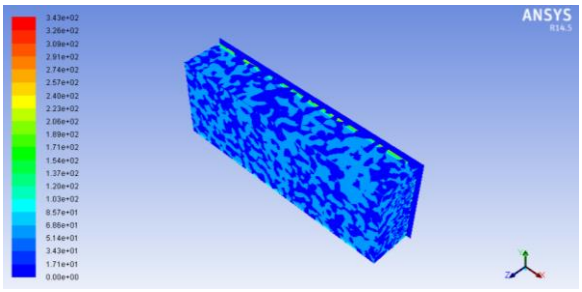

Figure 4.23 Absorbed Visible Solar Heat Flux distribution while considering inlet temperature 10°C and 0.5 velocity (flat plate surface)

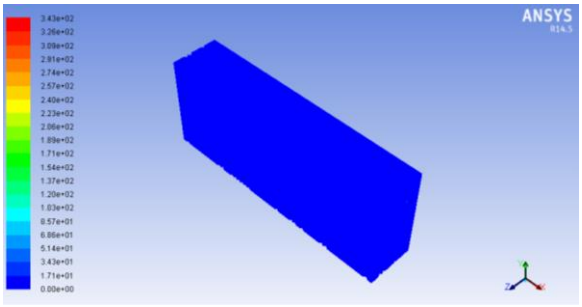

Figure 4.24 Absorbed Visible Solar Heat Flux distribution while considering inlet temperature 20°C and 0.5 velocity (flat plate surface)

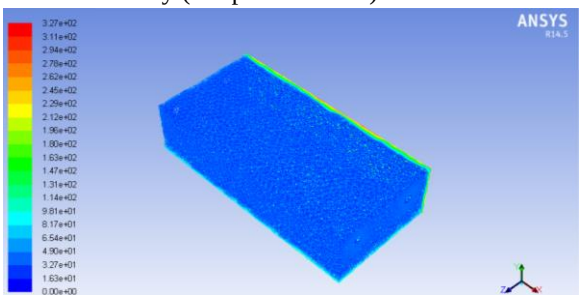

Figure 4.25 Absorbed Visible Solar Heat Flux distribution while considering inlet temperature 0°C and 0.5 velocity (art roughened surface)

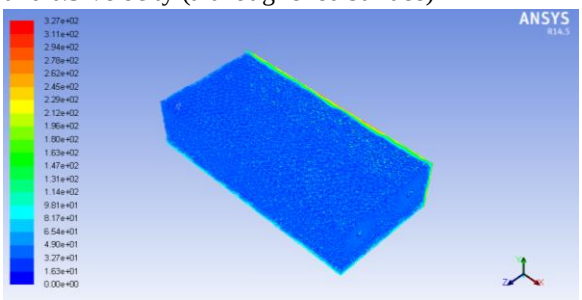

Figure 4.26 Absorbed Visible Solar Heat Flux distribution while considering inlet temperature 10°C and 0.5 velocity (art roughened surface)

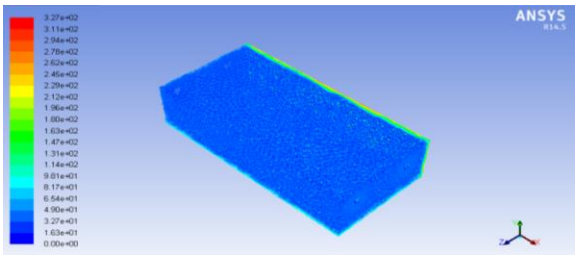

Figure 4.27 Absorbed Visible Solar Heat Flux distribution while considering inlet temperature 20°C and 0.5 velocity (art roughened surface)

Table 4.4 Relation between Absorbed Solar Heat Flux (W/m^2) (for Art Roughened and flat plate Surface) and Air inlet temperature

Air Inlet temperature (K)	Absorbed Solar Heat Flux (W/m^2) (Art Roughened Surface)	Absorbed Solar Heat Flux (W/m^2) (Flat Plate Surface)
273	326.87	342.91
283	326.87	342.91
293	326.87	342.91

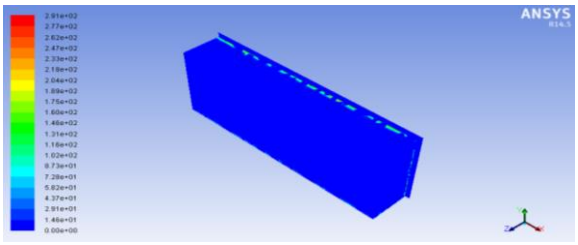

Figure 4.28 Absorbed IR Solar Heat Flux distribution while considering inlet temperature 0°C and 0.5 velocity (flat plate surface)

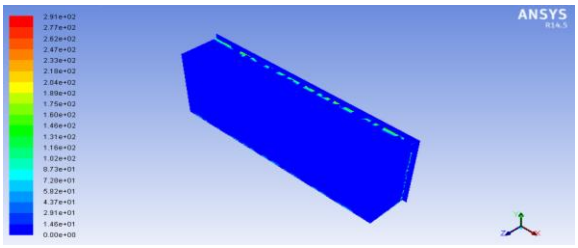

Figure 4.29 Absorbed IR Solar Heat Flux distribution while considering inlet temperature 10°C and 0.5 velocity (flat plate surface)

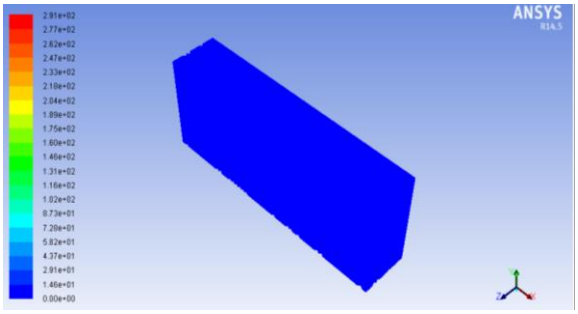

Figure 4.30 Absorbed IR Solar Heat Flux distribution while considering inlet temperature 20°C and 0.5 velocity (flat plate surface)

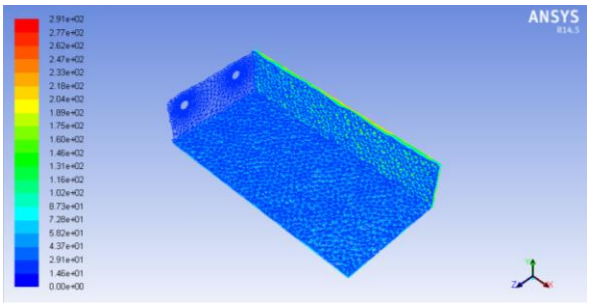

Figure 4.31 Absorbed IR Solar Heat Flux distribution while considering inlet temperature 0°C and 0.5 velocity (art roughened surface)

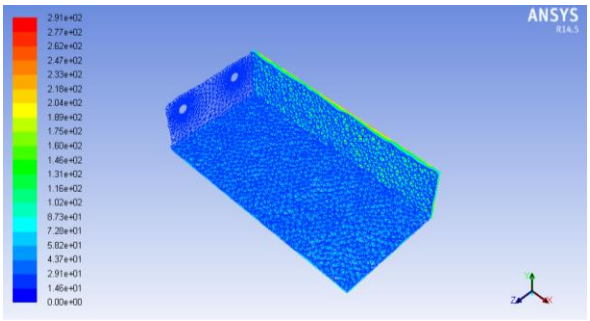

Figure 4.32 Absorbed IR Solar Heat Flux distribution while considering inlet temperature 10°C and 0.5 velocity (art roughened surface)

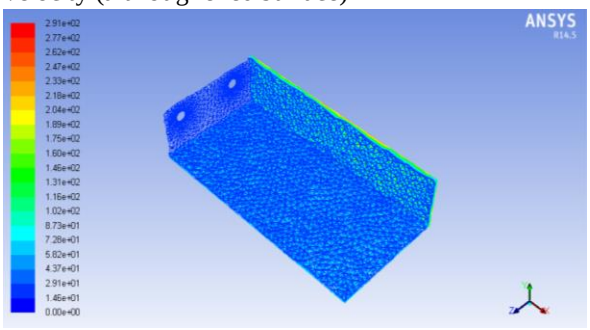

Figure 4.33 Absorbed IR Solar Heat Flux distribution while considering inlet temperature 20°C and 0.5 velocity (art roughened surface)

Table 4.5 Relation between Absorbed IR Solar Heat Flux (W/m^2) (for Art Roughened and flat plate Surface) and Air inlet temperature

Air Inlet temperature (K)	Absorbed IR Solar Heat Flux (W/m^2) (Art Roughened Surface)	Absorbed IR Solar Heat Flux (W/m^2) (Flat Plate Surface)
273	291.1033	291.1033
283	291.1033	291.1033
293	291.1033	291.1033

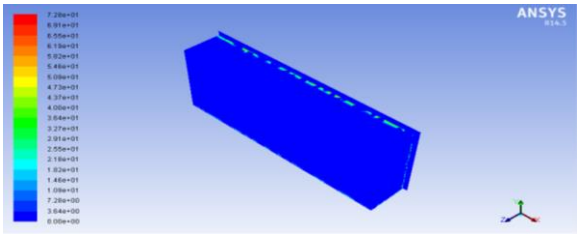

Figure 4.34 Reflected Visible Solar Heat Flux distribution while considering inlet temperature 0°C and 0.5 velocity (flat plate surface)

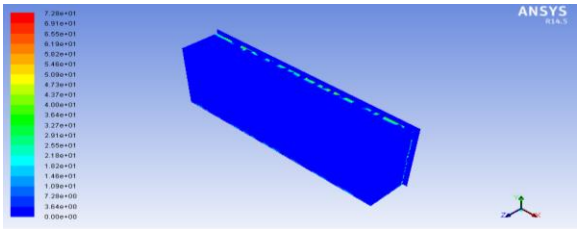

Figure 4.35 Reflected Visible Solar Heat Flux distribution while considering inlet temperature 10°C and 0.5 velocity (flat plate surface)

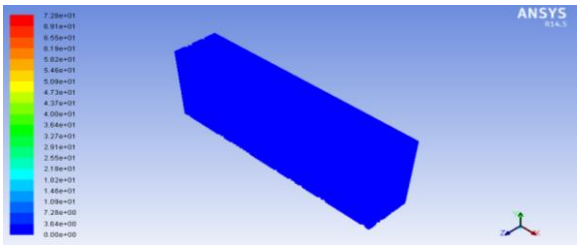

Figure 4.36 Reflected Visible Solar Heat Flux distribution while considering inlet temperature 20°C and 0.5 velocity (flat plate surface)

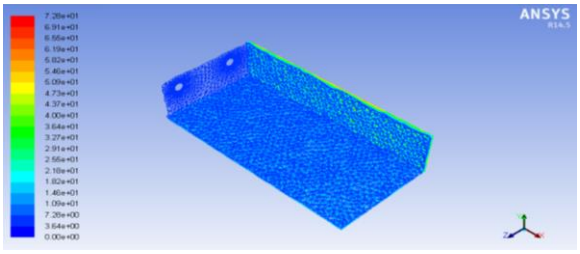

Figure 4.37 Reflected Visible Solar Heat Flux distribution while considering inlet temperature 0°C and 0.5 velocity (art roughened surface)

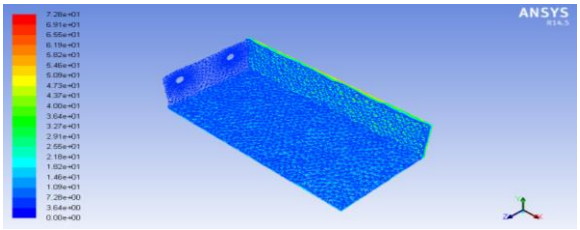

Figure 4.38 Reflected Visible Solar Heat Flux distribution while considering inlet temperature 10°C and 0.5 velocity (art roughened surface)

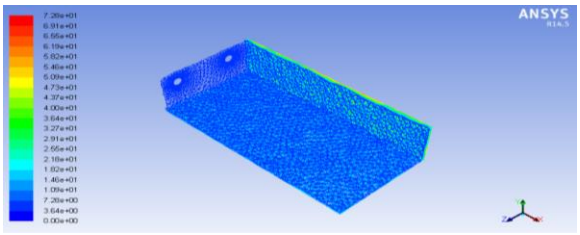

Figure 4.39 Reflected Visible Solar Heat Flux distribution while considering inlet temperature 20°C and 0.5 velocity (art roughened surface)

Table 4.6 Relation between Reflected Solar Heat Flux (W/m^2) (for Art Roughened and flat plate Surface) and Air inlet temperature

Air Inlet temperature (K)	Reflected Solar Heat Flux (W/m^2) (Art Roughened Surface)	Reflected Solar Heat Flux (W/m^2) (Flat Plate Surface)
273	72.8	72.8
283	72.8	72.8
293	72.8	72.8

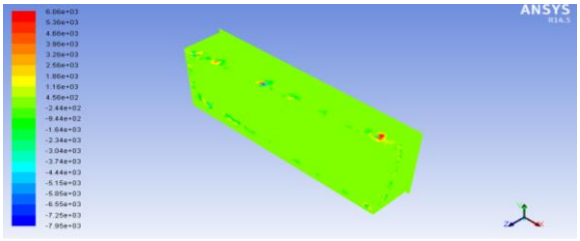

Figure 4.39 Surface Heat Transfer Coefficient distribution while considering inlet temperature 0°C and 0.5 velocity (flat plate surface)

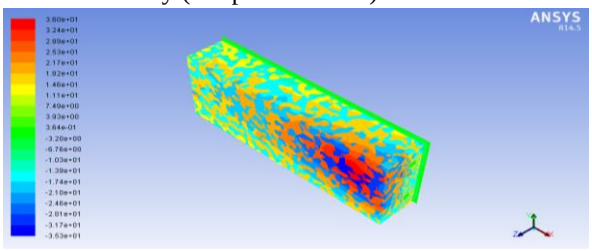

Figure 4.40 Surface Heat Transfer Coefficient distribution while considering inlet temperature 10°C and 0.5 velocity (flat plate surface)

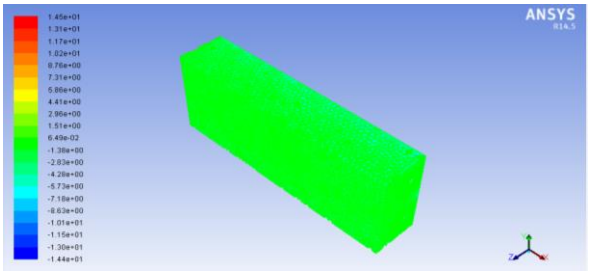

Figure 4.41 Surface Heat Transfer Coefficient distribution while considering inlet temperature 20°C and 0.5 velocity (flat plate surface)

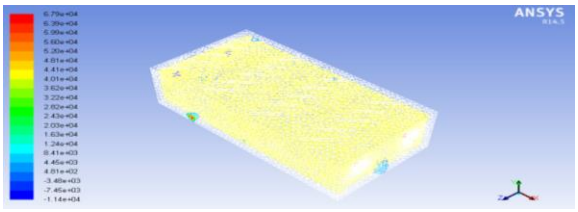

Figure 4.42 Surface Heat Transfer Coefficient distribution while considering inlet temperature 0°C and 0.5 velocity (art roughened surface)

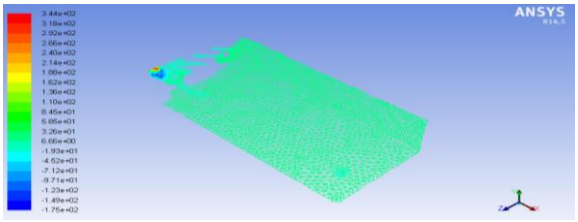

Figure 4.43 Surface Heat Transfer Coefficient distribution while considering inlet temperature 10°C and 0.5 velocity (art roughened surface)

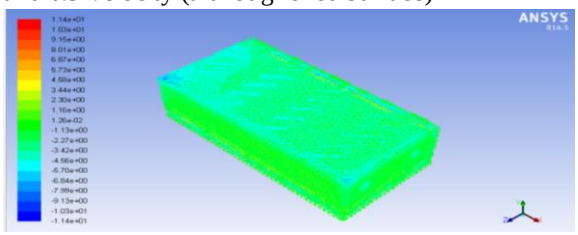

Figure 4.44 Surface Heat Transfer Coefficient distribution while considering inlet temperature 20°C and 0.5 velocity (art roughened surface)

Table 4.7 Relation between Surface Heat Transfer Coefficient (W/m^2k) (for Art Roughened and flat plate Surface) and Air inlet temperature

Air Inlet temperature (K)	Surface Heat Transfer Coefficient (W/m^2k) (Art Roughened Surface)	Reflected IR Solar Heat Flux (W/m^2k) (Flat Plate Surface)
273	67870	60574
283	343.92	359.88
293	11.439	14.548

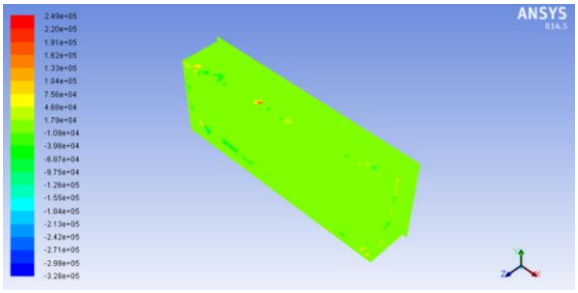

Figure 4.45 Surface Nusselt Number distribution while considering inlet temperature 0°C and 0.5 velocity (flat plate surface)

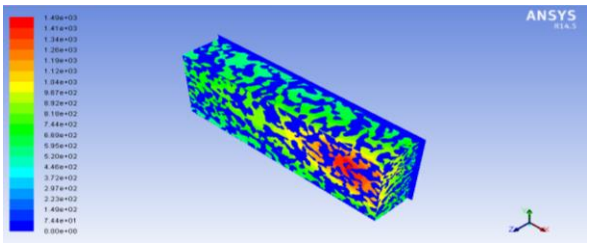

Figure 4.46 Surface Nusselt Number distribution while considering inlet temperature 10°C and 0.5 velocity (flat plate surface)

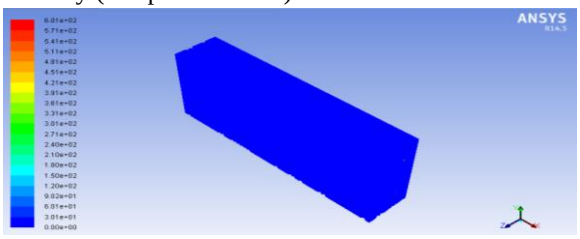

Figure 4.47 Surface Nusselt Number distribution while considering inlet temperature 20°C and 0.5 velocity (flat plate surface)

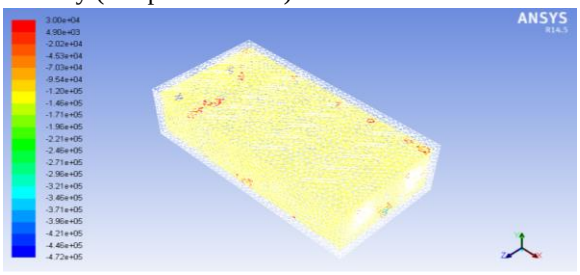

Figure 4.48 Surface Nusselt Number distribution while considering inlet temperature 0°C and 0.5 velocity (art roughened surface)

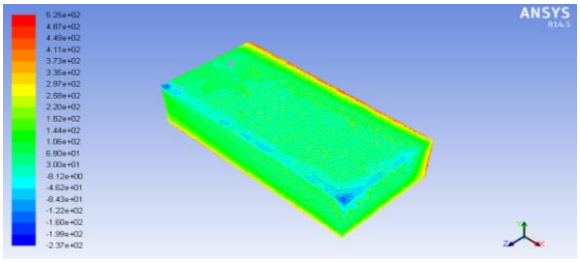

Figure 4.49 Surface Nusselt Number distribution while considering inlet temperature 10°C and 0.5 velocity (art roughened surface)

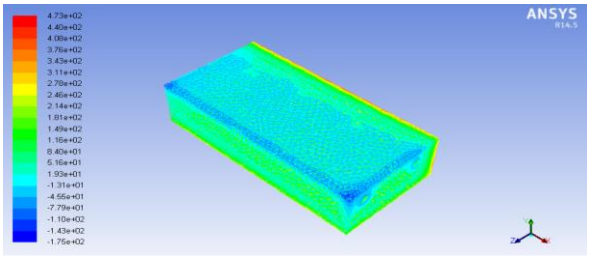

Figure 4.50 Surface Nusselt Number distribution while considering inlet temperature 20°C and 0.5 velocity (art roughened surface)

Table 4.8 Relation between Surface Nusselt Number (for Art Roughened and flat plate Surface) and Air inlet temperature

Air Inlet temperature (K)	Surface Nusselt Number (Art Roughened Surface)	Surface Nusselt Number (Flat Plate Surface)
273	29974	24873.5
283	525.01	1487.14
293	472.72	601.18

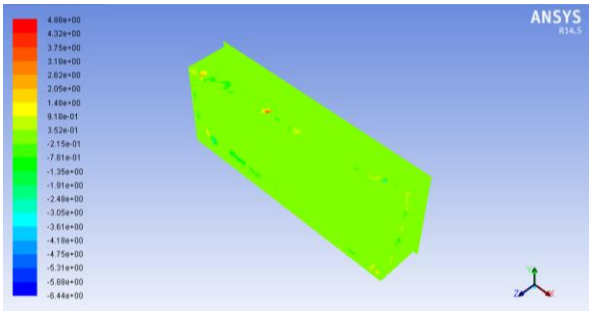

Figure 4.51 Surface Stanton Number distribution while considering inlet temperature 0°C and 0.5 velocity (flat plate surface)

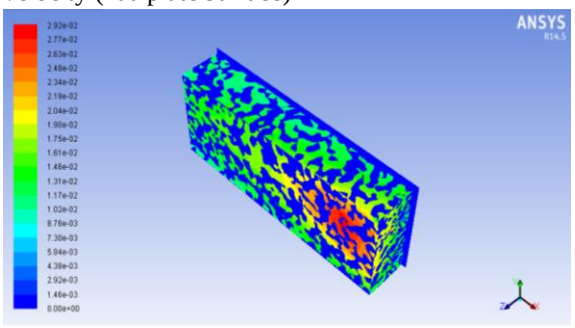

Figure 4.52 Surface Stanton Number distribution while considering inlet temperature 10°C and 0.5 velocity (flat plate surface)

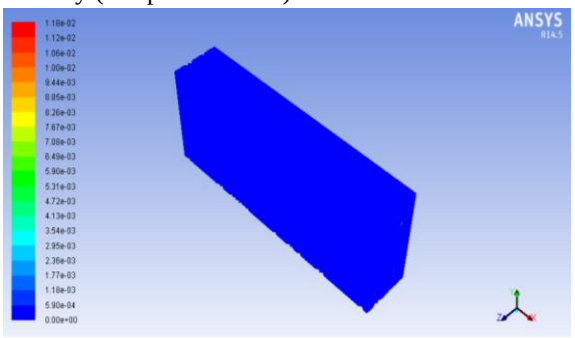

Figure 4.53 Surface Stanton Number distribution while considering inlet temperature 20°C and 0.5 velocity (flat plate surface)

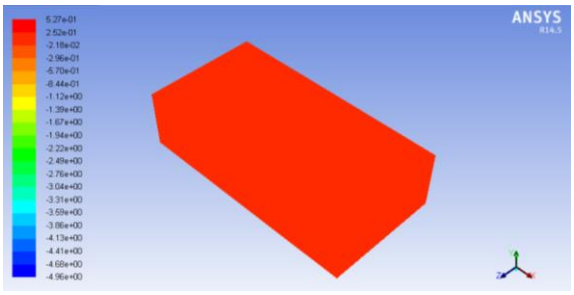

Figure 4.54 Surface Stanton Number distribution while considering inlet temperature 0°C and 0.5 velocity (art roughened surface)

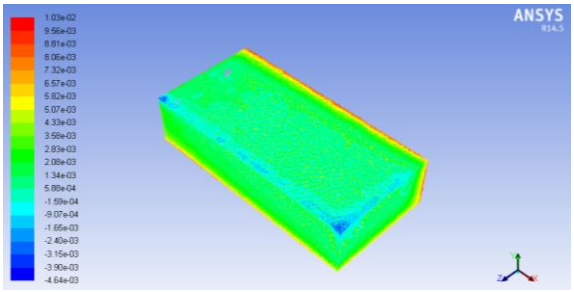

Figure 4.55 Surface Stanton Number distribution while considering inlet temperature 10°C and 0.5 velocity

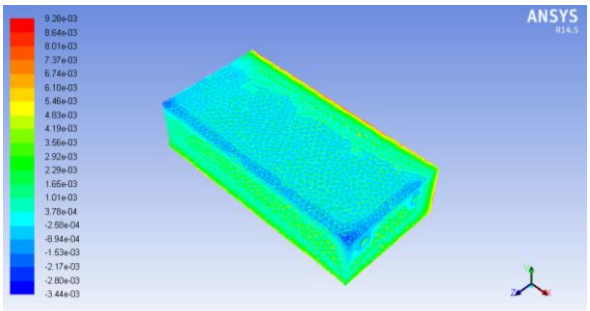

Figure 4.56 Surface Stanton Number distribution while considering inlet temperature 20°C and 0.5 velocity

Table 4.9 Relation between Surface Stanton Number (for Art Roughened and flat plate Surface) and Air inlet temperature

Air Inlet temperature (K)	Surface Stanton Number (Art Roughened Surface)	Surface Stanton Number (Flat Plate Surface)
273	0.528	0.488
283	0.0103	0.0291
293	0.00927	0.0118

4.2 Results considering varying wind velocity and constant inlet temperature

Table 4.10 shows the variation in Air outlet temperature with respect to inlet wind velocity.

Figure 4.20 shows the graph drawn between both the variables.

Table 4.10 Relation between air outlet temperature and wind velocity for Art Roughened and flat plate Surface

Wind Velocity (m/s)	Air outlet Temperature (K) (Art Roughened Surface)	Air outlet Temperature (K) (Flat Plate Surface)
1.0	334.59	325.2
1.5	334.98	325.45
2.0	335.68	325.65

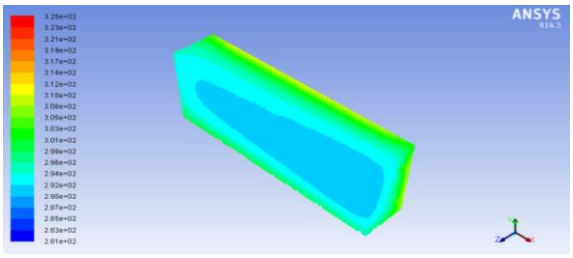

Figure 4.57 Temperature distribution while considering inlet temperature 10°C and 1.0 m/s velocity (Flat plate surface)

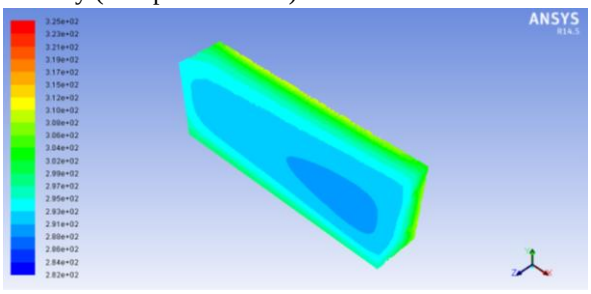

Figure 4.58 Temperature distribution while considering inlet temperature 10°C and 1.5 m/s velocity (Flat plate surface)

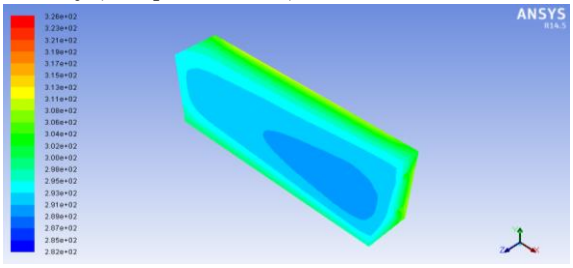

Figure 4.59 Temperature distribution while considering inlet temperature 10°C and 2.0 m/s velocity (Flat plate surface)

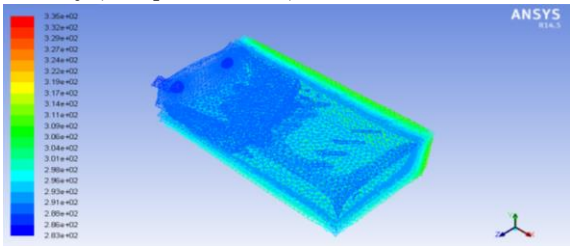

Figure 4.60 Temperature distribution while considering inlet temperature 10°C and 1.0 m/s velocity (art roughened surface)

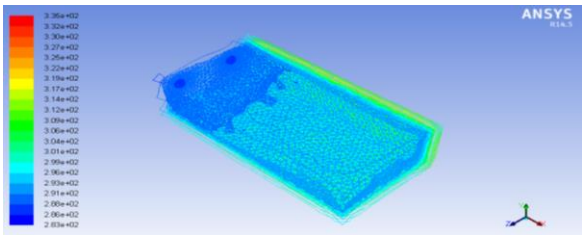

Figure 4.61 Temperature distribution while considering inlet temperature 10°C and 1.5 m/s velocity (art roughened surface)

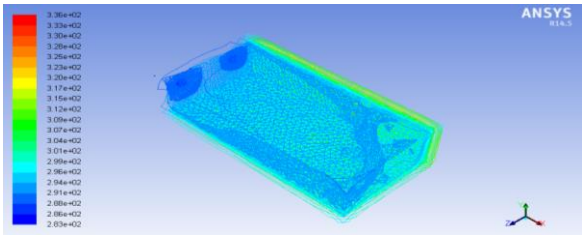

Figure 4.62 Temperature distribution while considering inlet temperature 10°C and 2.0 m/s velocity (art roughened surface)

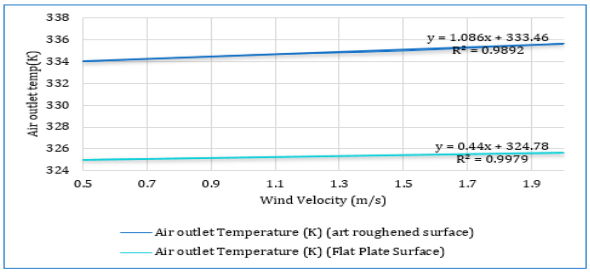

Figure 4.63 Relation between Air outlet temperature and Wind velocity

Table 4.11 Relation between Turbulent Kinetic Energy /Turbulence (m²/s²) and wind velocity for Art Roughened and flat plate Surface

Wind Velocity (m/s)	Turbulent Kinetic Energy/ Turbulence (m²/s²) (Art Roughened Surface)	Turbulent Kinetic Energy/ Turbulence (m²/s²) (Flat Plate Surface)
1.0	611.75	637.3
1.5	1168.23	1125
2.0	1861.7	1436

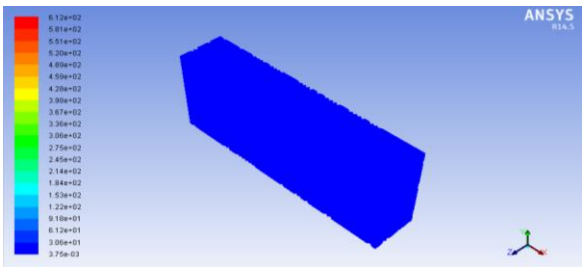

Figure 4.64 Turbulence distribution while considering inlet temperature 10°C and 1.0 m/s velocity (flat plate surface)

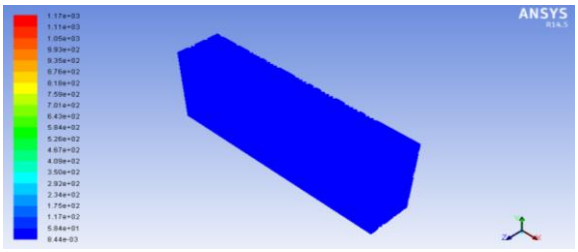

Figure 4.65 Turbulence distribution while considering inlet temperature 10°C and 1.5 m/s velocity (flat plate surface)

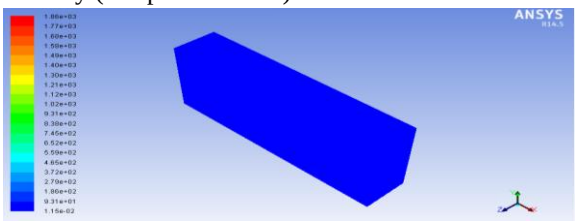

Figure 4.66 Turbulence distribution while considering inlet temperature 10°C and 2.0 m/s velocity (flat plate surface)

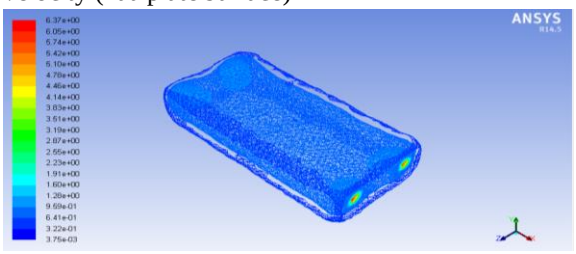

Figure 4.67 Turbulence distribution while considering inlet temperature 10°C and 1.0 m/s velocity (art roughened surface)

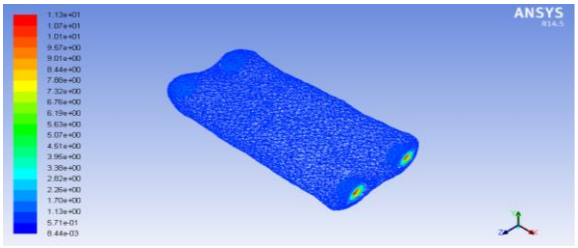

Figure 4.68 Turbulence distribution while considering inlet temperature 10°C and 1.5 m/s velocity

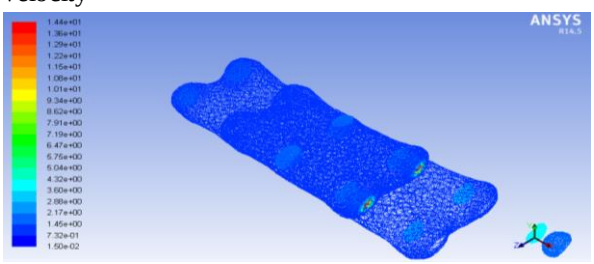

Figure4.69 Turbulence distribution while considering inlet temperature 10°C and 2.0 m/s velocity

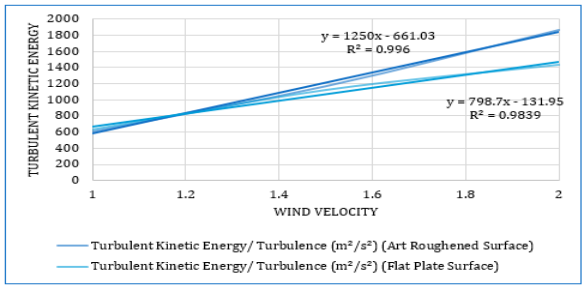

Figure 4.70 Relation between Turbulent Kinetic Energy and Wind velocity

5 CONCLUSION

In this present investigation, a numerical prediction has been conducted to study inlet velocity and temperature of air in two different type of solar air heater having the flat plate and artificial roughened absorber plate surface.

A comparative Finite element analysis has been carried out for air at different velocity (inlet) and temperature of fluid for both the condition.

The following are the important out comes of the present Finite Element analysis which represents the *artificial roughened surface is more suitable then the flat plate surface solar air heater.*

- While having the same volume the outlet air temperature achieved is more in solar air heater having artificial roughness compare then without artificial roughness solar air heater.
- The turbulence intensity, also often referred to as turbulence level and used for showing the effects of turbulence. The turbulence is much lower in case of artificial roughened surface as compare with flat plate surface solar air heater due to the geometrical changes. While increasing the fluid inlet temperature the turbulence decreases in both the cases.
- In both the cases the radiative heat flux is almost same for particular inlet air temperature. But the flat plate surface shows more radiative heat flux compare then art roughened surface solar air heater. The radiative heat flux decreases while increasing the inlet air temperature
- For each and every temperature condition the flat plate solar air heater shows 342.91 W/m^2 absorbed heat flux while artificial roughened surface solar air heater shows the value of 326.87 W/m^2 absorbed solar heat flux.

- For each and every temperature condition the flat plate solar air heater and artificial roughened surface solar air heater shows the value of 291.1 W/m^2 absorbed IR solar heat flux.
- Flat plate solar air heater and artificial roughened surface solar air heater shows the value of 72.8 W/m^2 of reflected solar heat flux.
- The surface heat transfer decreases with increment of air inlet temperature. Higher value of 67870 W/m^2k value can be achieved in artificial roughened solar air heater at 0°C temperature.
- The higher value of Nusselt number is achieved in artificial roughened surface which indicates the high rate of heat transfer.
- Higher value of Stanton number can be achieved using artificial roughened surface when the inlet temperature of the air is lowest, which shows high value of heat transfer achieved.
- There is increment in air outlet temperature as wind velocity increases this is due to the fact that wind velocity increases the heat transfer through the radiation and convection, thus results in increment in air outlet temperature.
- Turbulence kinetic energy is the mean kinetic energy per unit mass associated with eddies in turbulent flow. There is increment in Turbulent Kinetic Energy as wind velocity increases. Turbulence is maximum in inlet and outlet zone of the SAH as shown in contours.

REFERENCES

[1] Anil Singh Yadav, J.L. Bhagoria, 2014, "A CFD based thermo-hydraulic performance analysis of an artificially roughened solar air heater having equilateral triangular sectioned rib roughness on the absorber plate", 2014, International Journal of Heat and Mass Transfer 70 (2014) 1016–1039

[2] Anil P. Singh, Varun, Siddhartha, "Effect of artificial roughness on heat transfer and friction characteristics having multiple arc shaped roughness element on the absorber plate", 2014, Solar Energy 105 (2014) 479–493

[3] A.R. Jaurker, J.S. Saini b, B.K. Gandhi , "Heat transfer and friction characteristics of rectangular solar air heater duct using rib-grooved artificial roughness", 2006, Solar Energy 80 (2006) 895–907

[4] Brij Bhushan, Ranjit Singh, "A review on methodology of artificial roughness used in duct of solar air heaters", 2010, Energy 35 (2010) 202–212

[5] Khushmeet Kumar, D.R. Prajapati, Sushant Samir, "Heat Transfer and Friction Factor Correlations Development for Solar Air Heater Duct Artificially Roughened with 'S' Shape Ribs", 2016, Experimental Thermal and Fluid Science (2016)

[6] L. Varshney, A.D. Gupta, "Performance prediction for solar air heater having rectangular sectioned tapered rib roughness using CFD", Thermal Science and Engineering Progress (2017)

[7] Li Shui-lian, Meng Xiang-rui, Wei Xin-li, "Heat transfer and friction factor correlations for solar air collectors with hemispherical protrusion artificial roughness on the absorber plate", 2015, Solar Energy 118 (2015) 460–468

[8] Mohitkumar G. Gabhane , Amarsingh B. Kanase-Patil , 2017,"Experimental analysis of double flow solar air heater with multiple C shape roughness", 2017, Solar Energy 155 (2017) 1411–1416

[9] R.P. Saini, Jitendra Verma, "Heat transfer and friction factor correlations for a duct having dimple-shape artificial roughness for solar air heaters", 2008, Energy 33 (2008) 1277– 1287

[10] Ravi Kant Ravi, R.P. Saini ,"Experimental investigation on performance of a double pass artificial roughened solar air heater duct having roughness elements of the combination of discrete multi V shaped and staggered ribs", 2016, Energy 116 (2016) 507-516

[11] R. Kant Ravi, R.P. Saini, "Nusselt number and friction factor correlations for forced convective type counter flow solar air heater having discrete multi V shaped and staggered rib roughness on both sides of the absorber plate", Applied Thermal Engineering (2017)

[12] S.K. Saini a, R.P. Saini, 2008, "Development of correlations for Nusselt number and friction factor for solar air heater with roughened duct having arc-shaped wire as artificial roughness", 2008,

[13] Sharad Kumar, R.P. Saini, "CFD based performance analysis of a solar air heater duct provided with artificial roughness", 2009, Renewable Energy 34 (2009) 1285–1291

[14] Tabish Alam, Man-Hoe Kim, "A critical review on artificial roughness provided in rectangular solar air heater duct", 2017 Renewable and Sustainable Energy Reviews 69 (2017) 387–400

[15] Thakur Sanjay Kumar et al. "Use of artificial roughness to enhance heat transfer in solar air heaters – a review", 2010, , Journal of Energy in Southern Africa , Vol 21 No 1 , February 2010

[16] Varun, Amar Patnaik, R.P. Saini, S.K. Singal, Siddhartha, 2009, "Performance prediction of solar air heater having roughened duct provided with transverse and inclined ribs as artificial roughness", 2009, Renewable Energy 34 (2009) 2914–2922